The kinetics and dynamics of the multichannel multiwell reaction of CO($^1\Sigma^+$) with OH($^2\Pi$): theoretical investigation

Marziyeh Sadat Masoumpour[1] · Marzieh Daryanavard[1]

Abstract

The kinetics and mechanism of the gas-phase reaction between carbon monoxide and hydroxyl radical have been theoretically investigated on the lowest potential energy surface. The dynamics of the reaction of CO($^1\Sigma^+$) with OH($^2\Pi$) is studied by stochastic one-dimensional chemical master equation (CEM) simulation method. The role of the energized intermediates on the kinetics of the reaction was investigated by determination the fraction of different intermediates and products at the early stages of the reaction. The temperature dependence of the rate constants of the each individual channels of the reaction over a wide range of temperature (200–2000 K) was studied. The calculated rate constants from the CEM simulation were compared with those obtained from the RRKM–SSA [Rice–Ramsperger–Kassel–Marcus (RRKM) theory and Steady State Approximation (SSA)] method based on strong collision assumption. At lower temperatures, the calculated RRKM–SSA rate constant was found to be twice of the calculated by CEM, although the results are in good agreement with experimental values.

Keywords Atmospheric chemistry · Kinetics · Chemical master equation · Multichannel multiwell reaction

1 Introduction

The gas phase reaction of the hydroxyl radical with carbon monoxide is a crucial reaction in the combustion and atmospheric chemistry. This reaction is an important component of the hydrocarbon combustion models since it contributes to the propagation of hydrogen atom and constitutes the main source of CO_2 [1]. Further, the OH + CO reaction plays a central role in the atmospheric chemistry. This reaction is one of the important mechanisms of loss for tropospheric carbon monoxide and a remarkable source of ozone and CO_2 (through the HO_2 radical formed by the product hydrogen and molecular oxygen) [2]. In the lower atmosphere, this reaction is also the key reaction to control the concentration of the important OH free radical, which is involved in the stratospheric cycles to produce ozone and NO_x molecules.

Extensive experimental [3–31] and theoretical [32–53] investigations have been carried out for the OH + CO → H + CO_2 reaction. Thermal rate constants, k(T), have been determined experimentally in an extended temperature and pressure range [24]. The thermal rate constants values for this reaction show a strong non-Arrhenius dependence on temperature. They are nearly independent of T at low temperature (below 500 K). On the contrary, they sharply increase with T at temperatures higher than 500 K. The slope of the Arrhenius plot increases significantly at the higher temperatures than 500 K, which indicates that the actual energy barrier exists when the quantum mechanical tunnelling becomes less

✉ Marziyeh Sadat Masoumpour, masompour@gmail.com | [1]Department of Chemistry, Estahban Higher Education Center, Estahban 74519-44655, Iran.

important. The unusual temperature dependence of the rate constant for this reaction could be explained if it proceeds *via* the formation of an energized intermediate, HOCO radical, which could then dissociate either back to the original reactants or to the reaction products, $H + CO_2$, and could also be stabilized by collisions. The HOCO intermediate has been experimentally observed in several previous studies [10, 54–58]. Smith and Zellner [10] were the first to purpose that the reaction mechanism involved the formation of HOCO intermediate. Experiments have also determined the isotopic substitution of OD in OH [22, 28] and ^{17}O, ^{18}O and ^{13}C for CO [28].

The reaction system is small enough to be applied for the accurate quantum mechanical methods. Therefore, it has become a benchmark for kinetics and dynamics calculations. Energies of the important points on the potential energy surface have been calculated at different levels of theory by many research groups [44, 45, 50, 51, 59–69]. Several ab initio potential energy surface (PES) studies report existence of two intermediates, HOCO and HCO_2, which form in the reaction system. It is understood that, unlike ordinary bimolecular reactions, the reaction of CO with OH proceeds through the chemically activated intermediate HOCO. The RRKM rate constants have been calculated based on the results of these quantum mechanical calculations [24, 38, 40, 66, 68–72]. Zhu et al. [66] carried out an RRKM/master equation analysis using G2M potential energy surface and concluded that tunnelling may be responsible for the large values of rate constants at low tempratures. Senosian et al. [70] also calculated the RRKM/master equation rate constants by CCSD(T)/cc-pVTZ potential energy surface of Yu et al. [65]. In contrast to Zhu et al. [66], they concluded that tunnelling has < 10% contribution to reaction rate at 298 K and reproduced the experimental data over the temperature range 80–250 K but their results lower than experimental data, below 250 K. Rate constants have also been obtained using the methods of quantum reactive scattering [33, 34, 36, 37, 39, 53]. Further, quasiclassical trajectory calculations (QCT) have been carried out, usually on analytical surfaces derived from ab initio calculations [32, 41, 43, 49, 61, 73]. In general, thermal rate constant using QCT technique agree well with experimental data when the temperature is above 1000 K but are significantly underestimated below 1000 K, where the measured rate constant falls slowly with temperature. This defect may be attributed to the neglecting of tunnelling corrections.

For multichannel reactions consisting of deep potential wells, as the title reaction, it would be more accurate to look at the kinetics of each channel in the presence of other channels. Although the reaction has been the subject of many studies, to the best of our knowledge no theoretical data on the kinetics of the title multichannel

multiwell reaction considered such a technique in calculating the rate constants for each individual channels of this reaction. The pre-reaction van der Waals complexes and energized intermediates along the reaction coordinate is detected and their effect on the dynamics of the title reaction is investigated. In the present study, the dynamics of the reaction is investigated using the chemical master equation which describes the evolution of a network of the chemical reactions as a stochastic process. Its solution yields the probabilities that the system has any given composition as a function of time. The calculated rate constants from CME modelling are compared with those obtained from the RRKM–SSA method [74], which is based on strong collision assumption and steady state approximation (SSA) for the formation of energized intermediates.

2 Computational methods

Gaussian09 program suite [75] was used to optimize the geometries of the stationary. The optimized geometries of the reactants, products, intermediates, and transition states were obtained using the M11 method in conjunction with the 6-311G** basis set. Grimme's three-body dispersion correction (GD3) [76] was used with S8 = 0.0 and SR6 = 1.619 (the optimized values for a similar M06-2X functional) to include the long-range dispersion interactions. Masunov et al. [77] used M11+GD3/6-311G** to construct the potential energy surface (PES) for the title reaction and compared their results with some high-level ab initio values such as CCSD(T)-F12, CCSD(T) and MRCI//CAS. They found that the maximal deviation is approximately less than 3 kcal mol^{-1}. Single point calculations on the optimised M11 geometries at the CCSD(T) level along with the aug-cc-pVTZ basis set was carried out. The energies of stationary points, predicted in this work at CCSD(T)/aug-cc-pVTZ//M11+GD3/6-311G**, is reported in Table 1. The high level ab initio and CBS-QM11 level of theory values from the literature are also shown for compression. In addition, we assessed the multireference character of the species using the corresponding T1 diagnostic values [78] at the CCSD(T)/aug-cc-pVTZ//M11+GD3/6-311G** level of theory. The T1 values for the all stationary points in the PES (the reactants, products and transition states) of the title reaction are given in Table 2. The T1 diagnostic value for all structures except HCO_2 species, which according to our following discussion doesn't play an important role in kinetics and dynamics of this system, was found to be less than 0.03, indicating that single-reference calculations can be used reliably to characterize the present reactive system [78, 79]. Therefore, this method is sufficient accuracy to use for this system. Harmonic vibrational frequencies were obtained at the M11+GD3/6-311G** level of theory

Table 1 Relative energies (kJ mol^{-1}) for the critical points of PES, predicted at different levels of theory

Species	CCSD(T)// M11+GD3[a]	MRCI//CAS[b]	CCSD(T)[c]	CCSD(T)-F12[d]	CBS-QM11[f]
CO+OH	132.1			123.8	126.6
vdw1	123.8	112.9	116.8	114.3	117.5
vdw2	126.1	118.8	121.3	118.7	120.8
trans-HOCO	0	0	0	0	0
cis-HOCO	5.1	8.0	7.8	7.4	9.4
HCO$_2$	78.5			66.7	74.8
CO$_2$+H	29.9			29.2	25.9
TS1	128.2	106.2	121.9	121.4	124.9
TS2	145.7	124.9	157.8	136.9	141.6
TS3	40.2	39.2	39.0	38.9	39.4
TS4	134.3	128.3	132.0	133.9	132.2
TS5	160.3	160.7	159.0	160.5	157.9
TS6	84.4			87.4	83.1

[a]This work
[b]Reference [66]
[c]Reference [65]
[d]Reference [80]
[f]Reference [77]

Table 2 The values of T1 diagnostics test for all species at the CCSD(T)/aug-cc-pVTZ//M11+GD3/6-311G** level of theory

Species	T1	Species	T1
CO	0.018	vdw2	0.024
OH	0.010	TS1	0.023
trans-HOCO	0.021	TS2	0.026
cis-HOCO	0.022	TS3	0.022
HCO$_2$	0.057	TS4	0.025
CO$_2$	0.018	TS5	0.026
vdw1	0.022	TS6	0.022

to characterize the stationary points as local minima or first order saddle points by the absence or presence of an imaginary frequency, respectively, and to obtain zero-point vibration energy (ZPE). Some of thermodynamic properties of the stationary points such as ZPE, relative Gibbs free energies, enthalpies and entropies at the M11+GD3/6-311G** level of theory listed in the Table S1 to the Supplementary Information. Furthermore, the connection of each transition state to the corresponding minima along the reaction paths was validated using intrinsic reaction coordinate (IRC) calculations at the same level of theory.

The dynamics of the title reaction is studied by solving the chemical master equation. The CME is an equation which determines the probabilities that the system has any certain composition as a function of time. The MultiWell program suite [81] was used to solve the CME

to describe the variation of the fractional population of different species of the system with time and calculate the rate constants and reaction yields. The Multiwell program employs Gillespie's stochastic simulation algorithm [82, 83] to solve one-dimensional CME. The unimolecular microcanonical rate constants are calculated according to the VTST and RRKM theory in the MultiWell program suite [84–87].

In this work, the calculated rate constant from CEM are compared with the values obtained from the RRKM–SSA method [74], which is the multichannel RRKM-method along with the steady state assumption (SSA) for the formation and consumption of energized intermediates.

3 Results and discussion

The obtained PES and optimized geometries of all the stationary points at the CCSD(T)/aug-cc-pVTZ// M11+GD3/6-311G** level of theory are shown in Figs. 1 and 2, respectively. The proposed mechanism for the title reaction is displayed in Scheme 1, where *w* is the collisional rate coefficient for the stabilization processes and the energized species are marked with "*" character. The different reaction pathways are characterized by the different colors for clarity in each figure. The vibrational term values and the moments of inertia for all species are listed in Table 3.
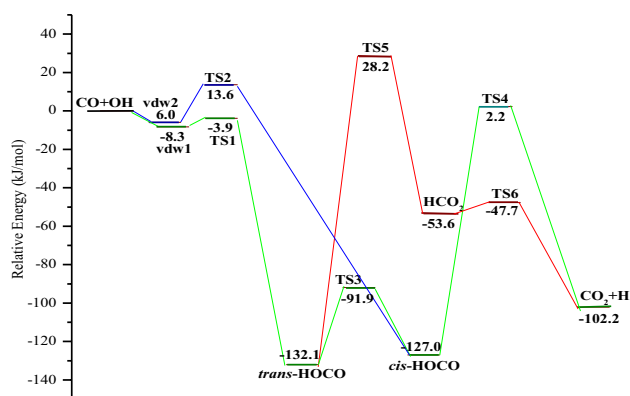
Fig. 1 The ZPE corrected relative energies for the reaction of CO($^1\Sigma^+$) with OH($^2\Pi$) at CCSD(T)/Aug-cc-pVTZ//M11+GD3/6-311G** level of theory. Three different energy pathways are presented by different colors

## 3.1 Some features of the potential energy surface and reaction mechanism

The lowest doublet PES for the reaction of CO($^1\Sigma^+$) and OH($^2\Pi$) at the CCSD(T)/aug-cc-pVTZ//M11+GD3/6-311G** level (Fig. 1) indicates that there are two entrance channels

for this system. The lowest energy pathway of the reaction (green color in Figs. 1, 2 and Scheme 1) consists the formation of a pre-reaction complex (vdw1), which is 8.3 kJ mol^{-1} more stable than the reactants. The vdw1 complex could undergo rearrangement process to form *trans*-HOCO intermediate, which is 132.1 kJ mol^{-1} more stable than the reactants by passing over a saddle point TS1 with low barrier height (4.4 kJ mol^{-1}, reaction R1). Internal rotation about the O–C bond in the chemically activated *trans*-HOCO can proceed *via* the gauche transition state, TS3, with torsional barrier of 40.2 kJ mol^{-1} to form an energized intermediate, *cis*-HOCO conformer that is 127.0 kJ mol^{-1} more stable than reactants (reaction R3). *cis*-HOCO conformer can also be produced from another entrance channel, intermediate energy pathway (blue color in Figs. 1, 2 and Scheme 1), via the pre-reaction hydrogen-bond van der Waals complex vdw2, which is 6.0 kJ mol^{-1} more stable than the reactants by passing over a saddle point TS2 with 19.6 kJ mol^{-1} barrier height (reaction R2). The energized *cis*-HOCO can convert to CO$_2$ molecule and hydrogen atom as the products, which are 102.0 kJ mol^{-1} more stable than the reactants by passing over or tunnelling through saddle point TS4 with 129.2 kJ mol^{-1} barrier height (reaction R4).

Fig. 2 The optimized structures of the stationary points at the M11+GD3/6-311G** level. Bond lengths are in angstrom and angles are in degree. According to the PES, green, blue and red arrows are the lowest, intermediate and highest energy pathways of the reaction of CO($^1\Sigma^+$) with OH($^2\Pi$), respectively
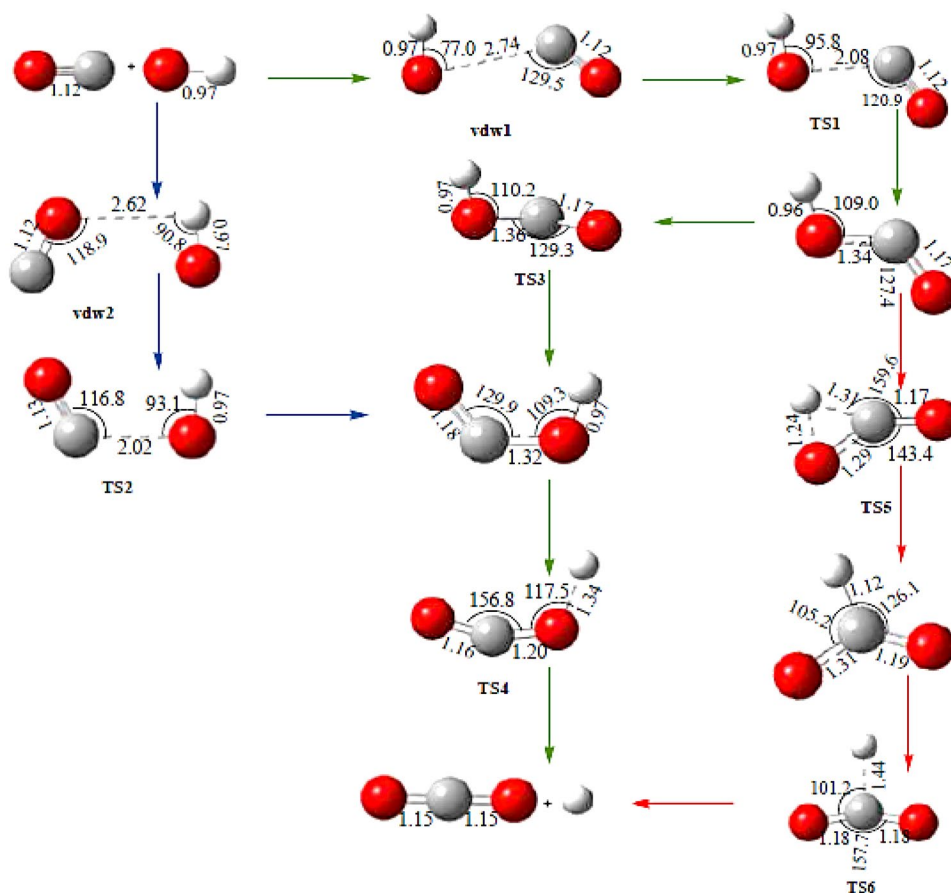
Scheme 1 The suggested mechanism for the reaction of $CO(^1\Sigma^+)$ with $OH(^2\Pi)$. The colors indicate the three different energy pathways of the reaction
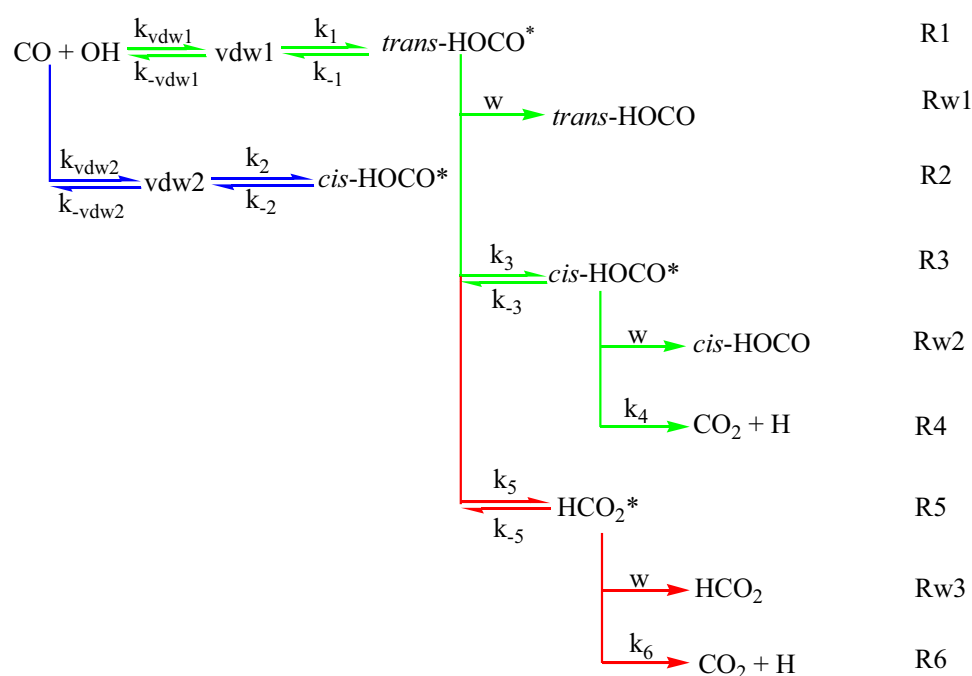
Table 3 The Harmonic vibrational wave numbers (cm^{-1}) and moments of inertia (amu $Å^2$) for the various species at the M11+GD3/6-311G** level of theory

Species	Wave numbers	I1, I2, I3
CO	2272.9	8.6
OH	3757.8	0.9
trans-HOCO	3875.4, 1972.0, 1235.5, 1110.9, 635.0, 566.8	3.0, 43.8, 46.8
cis-HOCO	3705.0, 1929.9, 1293.2, 1117.1, 619.7, 616.1	3.6, 42.3, 45.9
HCO_2	2848.0, 1814.3, 1334.3, 1009.5, 997.0, 337.3	4.8, 40.8, 45.6
CO_2	2456.9, 1406.4, 684.3, 684.3	42.7
vdw1	3767.5, 2283.4, 267.3, 216.8, 129.52, 46.6	4.4, 112.4, 116.8
vdw2	3768.9, 2256.9, 246.4, 146, 9, 103.3, 61.4	8.5, 90.7, 99.2
TS1	3778.5, 2246.3, 682.6, 235.9, 232.5, 278.4i	4.8, 70.4, 75.2
TS2	3751.1, 2192.9, 771.5, 202.6, 25.0, 433.6i	5.7, 63.1, 68.8
TS3	3833.6, 1949.5, 1092.1, 975.0, 664.4, 609.5i	3.4, 44.7, 46.6
TS4	2241.1, 1358.7, 950.7, 671.2, 532.2, 1815.9i	2.2, 45.3, 47.5
TS5	2235.4, 1914.2, 1216.9, 700.1, 547.7, 1662.2i	2.5, 44.6, 47.1
TS6	2144.9, 1403.9, 856.9, 736.4, 553.7, 674.8i	3.0, 43.0, 46.0

In case of having enough energy, *trans*-HOCO energized intermediate, *via* the highest energy pathway of this system (red color in Figs. 1, 2 and Scheme 1), can surmount or tunnel through transition state TS5 (160.3 kJ mol⁻¹ barrier height) to form HCO_2 intermediate (reaction R5) with 53.6 kJ mol⁻¹ energy relative to the reactants that dissociate to CO_2 and H products (reaction R6) by tunneling or surmounting through saddle point TS6 with 5.9 kJ mol⁻¹ barrier height.

3.2 Calculations of the rate constants

MultiWell program by Barker et al. was used to estimate the population fractions of different species in this multi-channel multiwell system with time and calculate the rate coefficients of different channels. The Multiwell program suite solves CME according to Gillespie's stochastic simulation algorithm. The idea behind the Gillespie's algorithm is to simulate a chain of Markov processes by sampling the

probability distribution of the time elapsed since the last reaction, τ, and the probability that a specific reaction will occur at τ, such that any reaction occurring at τ has probability 1 [88]. A standard CME can be written as [89]

$$\frac{d\rho_i}{dt} = \omega \sum_j P_{ij}\rho_j - \omega\rho_i - k\rho_i + g_i$$

where ω is the frequency of collision (the Lennard-Jones potential was used in this study), P_{ij} is the transition probability of going from state j to i on collision and k_i is the total microcanonical rate constant for the isomerization or dissociation of ith state. The function P_{ij} should satisfy the detailed balance constraint and normalization. In the case of a multichannel process, k_i will be the sum of the rate constants of the individual channels. g_i is a value which shows the changing of the population of the given energy grain due to association from reactants or isomerization.

The MultiWell master equation code employs the Rice–Ramsperger–Kassel–Marcus (RRKM) theory to compute the energy-dependent microcanonical rate constants of the reactions with intrinsic energy barriers. This equation can be used to calculate the rate constants according to RRKM theoy

$$k(E) = \left[\frac{m^{\#}}{m} \frac{\sigma_{ext}}{\sigma_{ext}^{\#}} \right] \frac{g_e^{\#}}{g_e} \frac{1}{h} \frac{G^{\#}(E - E_0)}{\rho(E)}$$

where $m^{\#}$ and m are the number of the optical isomers, $\sigma_{ext}^{\#}$ and σ_{ext} are the external rotation symmetry numbers, $g_e^{\#}$ and g_e are the electronic state degeneracies of the transition state and reactant, respectively, h is Planck's constant, $G^{\#}(E - E_0)$ is the transition state sum of states, E is the internal energy of the energized reactant molecule and E_0 is the reaction threshold energy, the potential energy differences between reactant and activated complex of the reaction, and $\rho(E)$ is the density of states of the reactant molecules. The canonical transition state theory (TST) and tunnelling correction through an unsymmetrical Eckart potential barrier [90–92], which was parametrized in terms of the energy barriers (forward and reverse directions) and the imaginary frequency, are routine in Multiwell package. The sums and densities of states were computed using the Stein-Rabinovitch extension [93] of the Beyer–Swinehart algorithm [94] by DenSum program, which is implemented in the MultiWell program suite.

The master equation calculations were carried out using reduced mechanism to simulate the reaction. According to the PES and Scheme 1, the mechanism of the reaction consisted of three intermediates (trans-HOCO, cis-HOCO and HCO$_2$) and two set of products, which are connected by six reactions. The van der Waals complexes in the entrance channel (vdw1, vdw2) were neglected, because they are weakly bound and they have extremely short lifetimes. All isomerization reactions were treated as reversible, while the reactions to form bimolecular products were treated as irreversible.

The energy grain size of 10 cm^{-1} to a maximum 85,000 cm^{-1}, and nitrogen as the bath gas were chosen to solve the master equation. The simulations were performed using ten million trials of 10^3 to 10^6 collisions. Lennard-Jones parameters for N$_2$, collider gas, ($\sigma = 3.75$ Å and $\varepsilon/k_B = 82.0$ K) and intermediates ($\sigma = 4.1$ Å and $\varepsilon/k_B = 210.0$ K) were obtained by Hippler et al. [95] An exponential model with alpha (E) switching function was used for the collisions. It was assume that there is a statistical distribution of the energy inside the energized intermediates, because of the internal vibrational energy redistribution (IVR) in the energized species was faster than the unimolecular reactions.

The K-rotor is assumed to exchange energy freely with the other internal degrees of freedom when it was included in computing the sums and densities of states, while the degenerate two-dimensional external rotation is assumed to be inactive.

The rate constant for the recombination reaction at the high pressure limit can be calculated from detailed balance by using the equilibrium constant $K(T_{trans})$ at translational temperature, T_{trans}:

$$K(T_{trans}) = k_{rec,\infty}(T_{trans}) / k_{uni,\infty}$$

where $k_{rec,\infty}(T_{trans})$ and $k_{uni,\infty}$ are the high pressure limiting recombination (reactants $\rightarrow$ trans-HOCO or reactants $\rightarrow$ cis-HOCO) and the unimolecular decompositions (trans-HOCO $\rightarrow$ reactants or cis-HOCO $\rightarrow$ reactants) rate constants, respectively. In this study, the total rate constant for the recombination reaction is sum of the recombination rate constants of each entrance channel. To obtain the overall rate constants for producing each species, the relative population (fraction) f_i of that species at the end of the simulation is multiplied by $k_{rec,\infty}(T_{trans})$:

$$K(T_{trans}) = f_i \times k_{rec,\infty}(T_{trans})$$

The equilibrium constant $K(T_{trans})$ is calculated using the Thermo program (part of the MultiWell program), which uses the standard statistical mechanics formulas for the partition functions of the reactants (CO and OH) and intermediates. $k_{uni,\infty}$ and the relative population (fraction) values, f_i, were obtained using Multiwell program by solving the CME at the specific pressure and temperature.
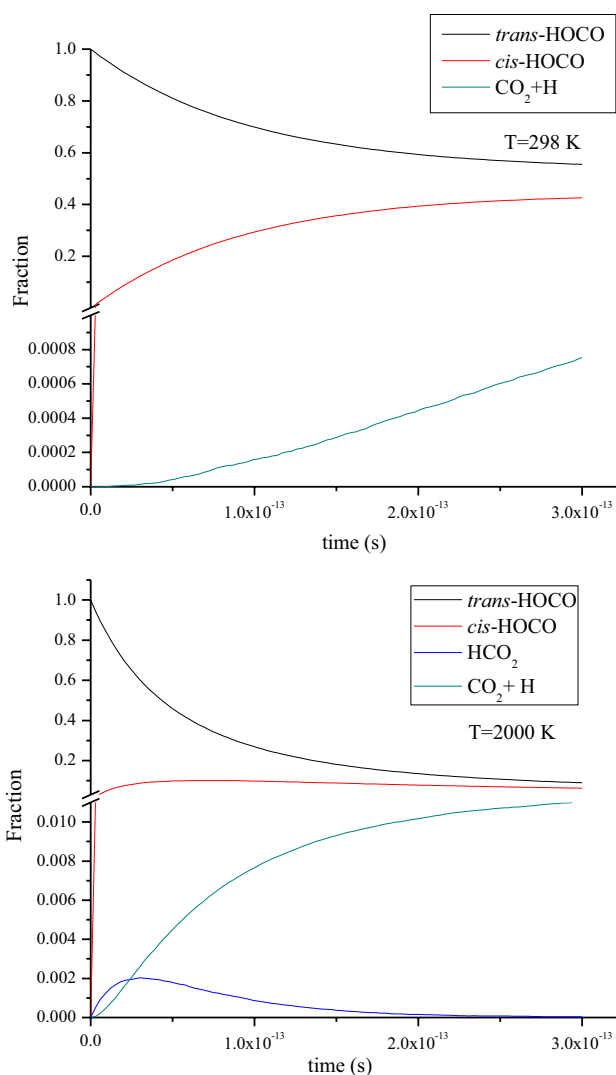
The population fractions of the different species in this reactive system at two different temperatures (298 and 2000 K) and reaction times (0.01–0.3 ps and 0.01–3 ns) are shown in Fig. 3 and 4. The feature of the PES along each particular channels is obviously determinant to judge
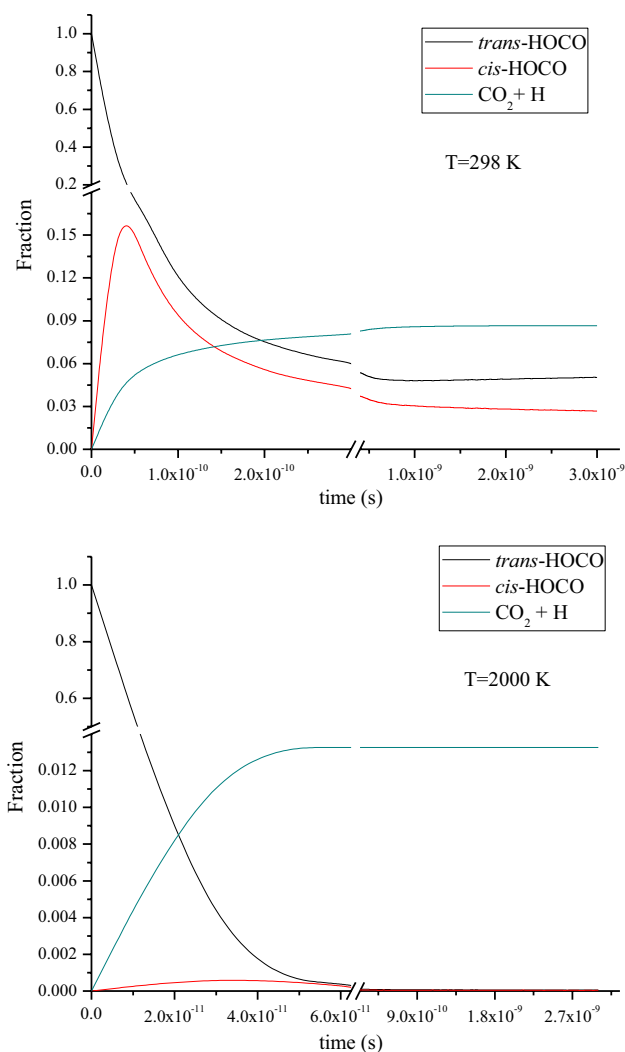
Fig. 3 The population fraction of the different species as a function of time at two different temperatures

Fig. 4 The population fraction of the different species as a function of time at early stages of the reaction (0.01–0.3 ps)

about the importance of each pathway in a complex system, confirming the fractional yields. According to the PES, formation of HCO_2 is the highest energy pathway of this system and it can be dissociated promptly to CO_2 and H products over the small barrier. Therefore, HCO_2 is a very short lifetime intermediate, which is only observed at the high temperatures at the early stages of the reaction, and it does not play an important role on the kinetics of this reaction. The decomposition of the HOCO intermediate competes with its stabilization at the moderate to high pressures. As shown in Figs. 3 and 4, because of the stabilization process at the higher temperatures is faster than low temperature, the population fraction of *trans*- and *cis*-HOCO are rapidly reached to Zero at 2000 K.

Owing the obtained results of the population fractions at different temperatures, the Arrhenius plots for different reaction channels at the early stages and long

reaction times are shown in Figs. 5 and 6, respectively. Figure 5 shows that the rate constants of formation of the intermediates are notable at the early stages of the reaction times (less than 10^{-13} s), while the intermediates are converted to the products at the longer reaction times (up to 10^{-9} s; Fig. 6).

The results indicate that in the long reaction time (about 3 ns), the population fractions of the energized intermediates are almost zero and products CO_2 and H are formed (Figs. 3, 6).

On the other hand, as shown in Fig. 5, the fraction and rate constant of *trans*-HOCO is high and the fraction and rate constant of the products ($CO_2 + H$) is low at the early stages of the reaction (up to 10^{-13} s). Meanwhile, in the time interval from 10^{-10} to 10^{-9} s, the fractional
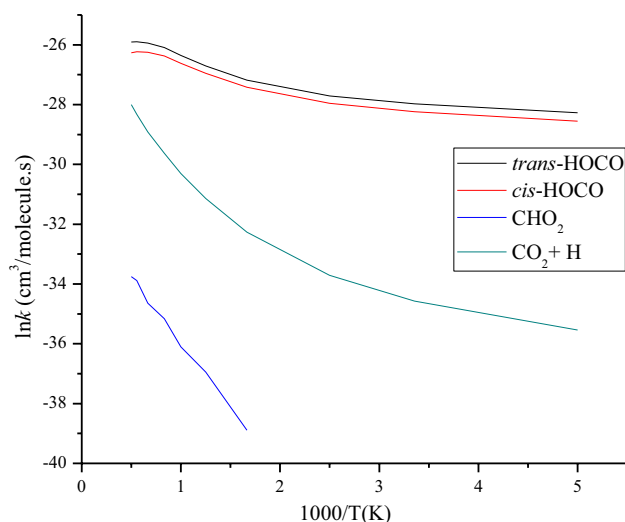
Fig. 5 Arrhenius plot for each individual channel of the reaction of CO + OH calculated using Multiwell program at the early stages of the reaction at early stages of the reaction (0.01–0.3 ps)
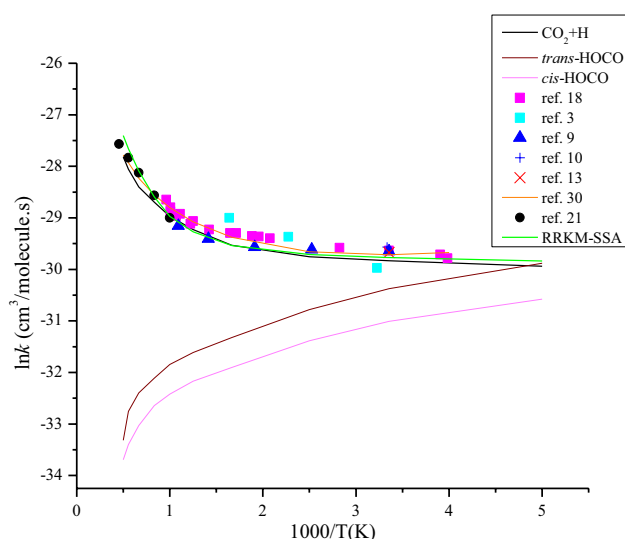
Fig. 6 Arrhenius plot for each individual channel of the reaction CO + OH calculated using Multiwell program at the longer reaction time (0.01–3 ns) and the RRKM–SSA method

population of product is increased and the fraction of intermediates approach to zero.

According to the experimental results [24, 50, 96], the thermal rate constants measured for a wide range of temperatures show a significant non-Arrhenius behaviour and the total rate constant shows no significant temperature dependence at low temperatures, which indicates that the quantum mechanical tunnelling plays an important role. Therefore, we calculated the rate constants with tunnelling correction through an unsymmetrical Eckart potential

barrier. As shown in Fig. 6, the obtained rate constants are in fairly good agreement with the experimental results. The following equation for the total rate expressions are obtained from fitting to the data in Fig. 6:

$$k_{CO_2+H} = 7.92 \times 10^{-19} T^{1.78} \exp\left(\frac{4.0 \text{ kJ mol}^{-1}}{RT}\right)$$

$$k_{trans-HOCO} = 1.64 \times 10^{-9} T^{-1.68} \exp\left(\frac{-1.4 \text{ kJ mol}^{-1}}{RT}\right)$$

$$k_{cis-HOCO} = 5.79 \times 10^{-10} T^{-1.60} \exp\left(\frac{-1.4 \text{ kJ mol}^{-1}}{RT}\right)$$

3.3 RRKM–SSA method

The rate of formation of the different reaction paths was also calculated using the RRKM–SSA method [74] according to a method suggested by Dean [97], which is based on a strong collision assumption. The results were then compared with those calculated by solving the CEM using Multiwell program.

The density of states of the reactant, the sum of states of the transition state along the reaction coordinates and the unimolecular rates for crossing various transition states were calculated using the RRKM program of Zhu and Hase [98]. In RRKM calculations, a step size of 0.4 kJ mol^{-1} (ΔE^+) was used to calculate the available energy for the activated complexes, and the external rotations were treated as adiabatic. N$_2$ was chosen as bath gas with a value of 0.5 for the collision [99]. To calculate the sums and densities of states, the semiclassical technique of Tardy, Whitten, and Rabinovitch [100], as implemented in the RRKM program, was used, in which the effective number of oscillators was adjusted as a function of the internal energy at each point along the reaction coordinate.

The individual rate constants for different channels and stabilization of each intermediate were calculated using the method based on the RRKM theory in conjugation with the steady state approximation (SSA) for energized intermediates [97]. The steady state approximation for the formation and consumption of the energized intermediates *trans*-HOCO, *cis*-HOCO and HCO$_2$ leads to the following expressions for the second order rate constants of Rw1, Rw2, Rw3, R4 and R6 reactions in the lower energy entrance channel (through vdw1) of this system (Scheme 1):

$$k_{bi}(R4)_{path1} = \kappa \frac{\sigma B_e Q_a}{h Q_{CO} Q_{OH}} \sum_{E_0}^{\infty} \frac{k_3(E) k_4(E) D''\{G(E^+)\} \exp(-E^+/RT)}{F}$$

$$k_{bi}(R6)_{path1} = \kappa \frac{\sigma B_e Q_a}{hQ_{CO}Q_{OH}} \sum_{E_0}^{\infty} \frac{k_5(E)k_6(E)D'\{G(E^+)\}\exp(-E^+/RT)}{F}$$

$$k_{bi}(Rw1)_{path1} = \frac{\sigma B_e Q_a}{hQ_{CO}Q_{OH}} \sum_{E_0}^{\infty} \frac{wD'D''\{G(E^+)\}\exp(-E^+/RT)}{F}$$

$$k_{bi}(Rw2)_{path1} = \frac{\sigma B_e Q_a}{hQ_{CO}Q_{OH}} \sum_{E_0}^{\infty} \frac{wk_3(E)D''\{G(E^+)\}\exp(-E^+/RT)}{F}$$

$$k_{bi}(Rw3)_{path1} = \frac{\sigma B_e Q_a}{hQ_{CO}Q_{OH}} \sum_{E_0}^{\infty} \frac{wk_5(E)D'\{G(E^+)\}\exp(-E^+/RT)}{F}$$

and the following expressions for the second-order rate constants of the reactions in the higher energy entrance channel (through vdw2) of this system:

$$k_{bi}(R4)_{path2} = \kappa \frac{\sigma B_e Q'_a}{hQ_{CO}Q_{OH}} \sum_{E_0}^{\infty} \frac{k_4(E)F'\{G(E^+)\}\exp(-E^+/RT)}{D'F}$$

$$k_{bi}(R6)_{path2} = \kappa \frac{\sigma B_e Q'_a}{hQ_{CO}Q_{OH}} \sum_{E_0}^{\infty} \frac{k_5(E)k_6(E)k_{-3}(E)\{G(E^+)\}\exp(-E^+/RT)}{F}$$

$$k_{bi}(Rw1)_{path2} = \frac{\sigma B_e Q'_a}{hQ_{CO}Q_{OH}} \sum_{E_0}^{\infty} \frac{wk_{-3}(E)D''\{G(E^+)\}\exp(-E^+/RT)}{F}$$

$$k_{bi}(Rw2)_{path2} = \frac{\sigma B_e Q'_q}{hQ_{CO}Q_{OH}} \sum_{E_0}^{\infty} \frac{wF'\{G(E^+)\}\exp(-E^+/RT)}{D'F}$$

$$k_{bi}(Rw3)_{path2} = \frac{\sigma B_e Q'_a}{hQ_{CO}Q_{OH}} \sum_{E_0}^{\infty} \frac{wk_{-3}(E)k_5(E)\{G(E^+)\}\exp(-E^+/RT)}{F}$$

where

$$D = w + k'_{-1}(E) + k_3(E) + k_5(E)$$
$$D' = w + k'_{-2}(E) + k_{-3}(E) + k_4(E)$$
$$D'' = w + k'_{-5}(E) + k_6(E)$$
$$F = DD'D'' - D''k'_{-3}(E)k_3(E) - D'k_5(E)k_{-5}(E)$$
$$F' = DD'D'' - D'k_5(E)k_{-5}(E)$$

where $k_{bi}(Rw1)$, $k_{bi}(Rw2)$ and $k_{bi}(Rw3)$ are the rate coefficients for the stabilization of energized intermediates trans-HOCO, cis-HOCO and HCO_2 under collision at 1 atm N_2, respectively. $k_{bi}(R_x)$s are the rate constants of corresponding channels. h is Plank constant, σ is the reaction path degeneracy, Q_a and Q'_a are the products of translational and rotational partition functions of TS1 and TS2

respectively; Q_{CO} and Q_{OH} are the partition functions of the reactants. κ is the tunnelling factor according to a model suggested by Brown [101], where a hydrogen atom approaches to a one-dimensional unsymmetrical Eckart barrier. $G(E^+)$ is the sum of vibrational states of the corresponding transition states at internal energy E^+, w ($= Z\beta_c[M]$) is the collisional stabilization for energized intermediates, in which Z, β_c and [M] are the collision frequency, the collision efficiency and the total bath gas density, respectively, and $k_x(E)$s are the microcanonical rate constants for the corresponding steps in the energy range of E^+ and $E^+ + dE$, which is calculated from the quotient of the sum of states to density of states of the corresponding steps. B_e is the ratio of the electronic partition functions for two association reactions of entrance channels that was calculated as:

$$B_e = \frac{2}{2 + 2\exp(-1665.3/RT)}$$

According of the PES of this reaction, there are two pre-reaction van der Waals complexes (vdw1 and vdw2) in the entrance channel of the reaction. It was recognized long age that there are different dynamical methods to account multiple reflections above the van der Waals complexes wells along the reaction coordinates on the rate constant of the reactions [102–104]. In this work, we used the method based on the canonical ensembles, to calculate the effect of the multiple reflections above the pre-reaction complexes (vdw1 and vdw2) in the entrance reaction channel, which is introduced by Garrett et al. [104]. The general expression of canonical unified statistical (CUS) rate is given by:

$$k^{CUS} = k^{CVT}(T)R^{CUS}(T)$$

with

$$R^{CUS}(T) = \left[1 + \frac{k^{CVT}}{k^{max}} + \frac{k^{CVT}}{k^{min}}\right]^{-1}$$

where k^{CVT} (rate constant of the canonical variational transition state theory), k^{max} and k^{min} are calculated at the highest maximum of ΔG (near the saddle point), the second highest maximum, and the minimum of ΔG (lowest minima between two maxima), with all free energies measured with respect to the reactants, respectively. Therefore, $R^{CUS}(T)$ indicates a degree of the multiple reflection or recrossing effect. In our study, the CVT and CUS thermal rate constants are calculated using the POLYRATE

2016-2A program suite [105]. Our results show that the recrossing or multiple reflections above two van der Waals complex (vdw1 and vdw2) have a slight effect on the rate constants (a decrease in the rate constants by a factor of 0.97 at 1000 K, and 0.98 at 2000 K). It is assumed that before further progress of the reaction, the microcanonical equilibrium between the reactants and vdw1 or vdw2 is rapidly established. Therefore, the role of formation of the pre-reaction complexes vdw1 and vdw2 could be assumed to be negligible.
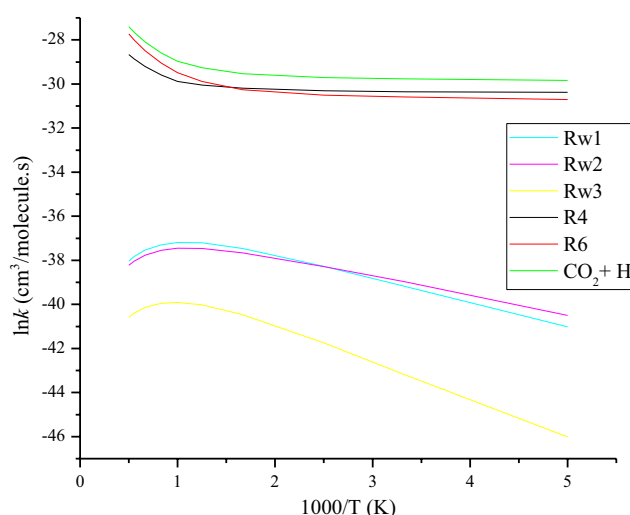
For each reaction channel, sum of the calculated rate constants of the reaction path1 (*via* vdw1) and path2 (*via* vdw2) are the total bimolecular rate constants. The Arrhenius plots for the reactions R4, R6, Rw1, Rw2, and Rw3 and the total rate constant for the formation of the products, CO_2 and H, (sum of the rate constants of the reactions R4 and R6) are shown in Fig. 7.

The following rate expressions are obtained from the non-linear least squares fitting the data in Fig. 7:

$$k_4 = 5.15 \times 10^{-19} T^{1.72} \exp\left(\frac{4.6 \text{ kJ mol}^{-1}}{RT}\right)$$

$$k_6 = 4.60 \times 10^{-22} T^{2.75} \exp\left(\frac{6.6 \text{ kJ mol}^{-1}}{RT}\right)$$

$$k_{CO_2+H} = 1.29 \times 10^{-20} T^{2.36} \exp\left(\frac{6.0 \text{ kJ mol}^{-1}}{RT}\right)$$

$$k_{Rw1} = 6.33 \times 10^{-10} T^{-2.08} \exp\left(\frac{-14.9 \text{ kJ mol}^{-1}}{RT}\right)$$

$$k_{Rw2} = 5.56 \times 10^{-11} T^{-1.81} \exp\left(\frac{-12.3 \text{ kJ mol}^{-1}}{RT}\right)$$

$$k_{Rw3} = 5.45 \times 10^{-10} T^{-2.35} \exp\left(\frac{-20.6 \text{ kJ mol}^{-1}}{RT}\right)$$

The calculated RRKM–SSA rate constant for the formation of CO_2 and hydrogen atom products is compared with that is obtained by solving the CME and the experimental results in Fig. 6. As shown in Fig. 6, there is a good agreement between the results of the RRKM–SSA and the CME methos especially at higher temperatures (beyond 500 K). At lower temperatures, beacuse of the strong collision asomption in the calculated RRKM–SSA rate constant which assume that the lifetime of the energized intermediates is long enough to make the energy distribution statistical and therefore overestimates the calculated rate constants of collisional stabilisation of the intermediates, it was found to be twice of that obtained by Multiwell program which employ the Lenard-Jones potential to simulate the collisions. However, the MultiWell program is based on the one-dimensional master equation, in which the active (randomizable) internal energy (E) is considered and it does not include the angular momentum (J) (the two-dimensional master equation). In order to obtain the more accurate results by the CEM method, the additional studies will be needed to model the title reaction with E–J resolved two-dimensional multiwell master equation to account for the centrifugal effects. It is worth mentioning that although a simple collision energy transfer model (strong assumption) was used in the RRKM–SSA method, the rate constants were obtained by including the effect of tunnelling through transition states and multiple reflections above the pre-reaction complexes.

4 Conclusions

We have studied the kinetics and dynamics of the reaction between carbon monoxide molecule, $CO(^1\Sigma^+)$, and hydroxyl radical, $OH(^2\Pi)$, by solving the stochastic CEM on the lowest doublet PES obtained at the CCSD(T)/aug-cc-pVTZ//M11+GD3/6-311G** level of theory. The suggested mechanism for the reaction consists of 9 different reactions with CO_2 and H as the major products. The change of population fraction of the key species in the system with time was studied at the early stages of reactions, where the fraction of the energized intermediates start to decrease and convert to the products. Furthermore, the

Fig. 7 Arrhenius plot for the various channels of the reaction of CO+OH in N_2 bath gas at 1 atm calculated using the RRKM–SSA method

population fraction of the key species of the title reaction obtained at longer reaction times over the temperature range from 200 to 2000 K. The results indicated that HCO_2 is an extremely short lifetime intermediate, which is form only at the early stages of the reaction at high temperatures. Therefore, it has not important role in the kinetics of the title reaction. The rate constants of each individual path is predicted by solving the chemical master equation and also RRKM–SSA method. Both methods predict the rate constant for the formation of the products of the title reaction in the reasonable agreement with the reported experimental data in the literature over the wide range of temperature (200–2000 K). The calculated rate constant by RRKM–SSA method with the strong collision assumption and therefore more effective energy transfer during the collisions, was compared with that obtained by solving the chemical master equation. According to strong collision assumption, it has been assume that the lifetime of the energized intermediates is long enough to make the energy distribution statistical. It should be note that this form of treatment in calculating the rate constants causes an overestimation of collisional stabilisation of the intermediates. Our results in this study are expected to have the costly modelling implication in the combustion and atmospheric chemistry.

Compliance with ethical standards

Conflict of interest There is no conflict of interest.

References

1. Warnatz J, Maas U, Dibble RW, Warnatz J (1996) Combustion. Springer, Heidelberg
2. Wayne R (2000) Chemistry of the atmosphere, 3rd edn. Oxford University Press, Oxford
3. Belles F, Potter AE Jr, Wong E (1967) Reaction rates of carbon monoxide with hydroxyl radicals and oxygen atoms. NASA Lewis Research Center, Cleveland
4. Greiner N (1969) Hydroxyl radical kinetics by kinetic spectroscopy. V. Reactions with H_2 and CO in the Range 300–500 K. J Chem Phys 51:5049–5051
5. Dean A, Kistiakowsky G (1971) Oxidation of carbon monoxide/methane mixtures in shock waves. J Chem Phys 54:1718–1725
6. Dryer F, Naegeli D, Glassman I (1971) Temperature dependence of the reaction $CO + OH -> CO_2 + H$. Combust Flame 17:270–272
7. Izod T, Kistiakowsky G, Matsuda S (1971) Oxidation of carbon monoxide mixtures with added ethane or azomethane studied in incident shock waves. J Chem Phys 55:4425–4432
8. Stuhl F, Niki H (1972) Pulsed vacuum-uv photochemical study of reactions of OH with H2, D2, and CO using a resonance-fluorescent detection method. J Chem Phys 57:3671–3677
9. Westenberg A, DeHaas N (1973) Rates of CO + OH and H_2 + OH over an extended temperature range. J Chem Phys 58:4061–4065
10. Smith IW, Zellner R (1973) Rate measurements of reactions of OH by resonance absorption. Part 2: reactions of OH with CO, C_2H_4 and C_2H_2. J Chem Soc Perkin Trans 2(69):1617–1627
11. Howard CJ, Evenson K (1974) Laser magnetic resonance study of the gas phase reactions of OH with CO, NO, and NO_2. J Chem Phys 61:1943–1952
12. Trainor DW, Vonrosenberg C Jr (1974) Energy partitioning in the reaction $OH + CO \rightarrow CO_2 + H$. Chem Phys Lett 29:35–38
13. Atkinson R, Baulch D, Cox R, Hampson R Jr, Kerr J, Rossi M, Troe J (1999) Evaluated kinetic and photochemical data for atmospheric chemistry, organic species: supplement VII. J Phys Chem Ref Data 28:191–393
14. Overend R, Paraskevopoulos G (1977) The question of a pressure effect in the reaction OH + CO at room temperature. Chem Phys Lett 49:109–111
15. Biermann H, Zetzsch C, Stuhl F (1978) On the pressure dependence of the reaction of HO with CO. Ber Bunsenges Phys Chem 82:633–639
16. Clyne MA, Holt PM (1979) Reaction kinetics involving ground $X^2\Pi$ and excited $A^2\Sigma^+$ hydroxyl radicals. Part 1. Quenching kinetics of OH $A^2\Sigma^+$ and rate constants for reactions of OH $X^2\Pi$ with CH_3CCl_3 and CO. J Chem Soc Perkin Trans 75:569–581
17. Paraskevopoulos G, Irwin RS (1982) The pressure dependence of the rate constant of the reaction of OD radicals with CO. Chem Phys Lett 93:138–143
18. Ravishankara A, Thompson R (1983) Kinetic study of the reaction of OH with CO from 250 to 1040 K. Chem Phys Lett 99:377–381
19. Jonah CD, Mulac WA, Zeglinski P (1984) Rate constants for the reaction of hydroxyl + carbon monoxide, hydroxyl-d + carbon monoxide, and hydroxyl + methane as a function of temperature. J Phys Chem 88:4100–4104
20. DeMore W (1984) Rate constant for the OH + CO reaction: pressure dependence and the effect of oxygen. Int J Chem Kinet 16:1187–1200
21. Wooldridge MS, Hanson RK, Bowman CT (1994) Shock tube study of the $CO + OH \rightarrow CO_2 + H$ reaction. In: Symposium (international) on combustion. Elsevier
22. Smith IW, Williams MD (1985) Kinetics of OH (v = 0 and 1) and OD (v = 0 and 1) studied by time-resolved laser-induced fluorescence. Ber Bunsenges Phys Chem 89:319–320
23. Ian W (1991) Vibrational-state distribution of CO_2 produced in the reaction between OH radicals and CO. J Chem Soc, Faraday Trans 87:1037–1038
24. Fulle D, Hamann H, Hippler H, Troe J (1996) High pressure range of addition reactions of HO. II. Temperature and pressure dependence of the reaction $HO + CO \Leftrightarrow HOCO \rightarrow H + CO_2$. J Chem Phys 105:983–1000
25. Golden D, Smith G, McEwen A, Yu CL, Eiteneer B, Frenklach M, Vaghjiani G, Ravishankara A, Tully F (1998) OH (OD) + CO: measurements and an optimized RRKM fit. J Phys Chem A 102:8598–8606
26. Röckmann T, Brenninkmeijer C, Saueressig G, Bergamaschi P, Crowley J, Fischer H, Crutzen P (1998) Mass-independent oxygen isotope fractionation in atmospheric CO as a result of the reaction CO + OH. Science 281:544–546
27. Feilberg KL, Sellevåg SR, Nielsen CJ, Griffith DW, Johnson MS (2002) $CO + OH \rightarrow CO_2 + H$: the relative reaction rate of five CO isotopologues. Phys Chem Chem Phys 4:4687–4693
28. Feilberg KL, Johnson MS, Nielsen CJ (2005) Relative rates of reaction of $^{13}C^{16}O$, $^{12}C^{18}O$, $^{12}C^{17}O$ and $^{13}C^{18}O$ with OH and OD radicals. Phys Chem Chem Phys 7:2318–2323

29. Joshi AV, Wang H (2006) Master equation modeling of wide range temperature and pressure dependence of $CO + OH \rightarrow$ products. Int J Chem Kinet 38:57–73

30. Li J, Zhao Z, Kazakov A, Chaos M, Dryer FL, Scire JJ Jr (2007) A comprehensive kinetic mechanism for CO, CH_2O, and CH_3OH combustion. Int J Chem Kinet 39:109–136

31. Laganà A, Garcia E, Paladini A, Casavecchia P, Balucani N (2012) The last mile of molecular reaction dynamics virtual experiments: the case of the OH (n = 1–10) + CO (j = 0–3) reaction. Faraday Discuss 157:415–436

32. Clary DC, Schatz GC (1993) Quantum and quasiclassical calculations on the $OH + CO \rightarrow CO_2 + H$ reaction. J Chem Phys 99:4578–4589

33. Hernández MI, Clary DC (1994) A study of HOCO resonances in the $OH + CO \rightarrow CO_2 + H$ reaction. J Chem Phys 101:2779–2784

34. Goldfield EM, Gray SK, Schatz GC (1995) Quantum dynamics of a planar model for the complex forming $OH + CO \rightarrow H + CO_2$ reaction. J Chem Phys 102:8807–8817

35. Zhang DH, Zhang JZ (1995) Quantum calculations of reaction probabilities for $HO + CO \rightarrow H + CO_2$ and bound states of HOCO. J Chem Phys 103:6512–6519

36. Balakrishnan N, Billing G (1996) A quantum-classical study of the reaction CO (v = 1, j = 1) + OH (v = 2, j = 2) $\rightarrow$ CO2 + H. J Chem Phys 104:4005–4011

37. Dzegilenko FN, Bowman JM (1998) "Spectator" modes in resonance-driven reactions: three-dimensional quantum calculations of HOCO resonances. J Chem Phys 108:511–518

38. Valero R, Kroes GJ (2002) Theoretical rate constants for the $OH + CO \rightarrow H + CO_2$ reaction using variational transition state theory on analytical potential energy surfaces. J Chem Phys 117:8736–8744

39. McCormack DA, Kroes GJ (2002) Full-dimensional quantal initial state-selected reaction probabilities (J = 0) for the reaction OH (v = 0, j = 0) + CO (v = 0, j = 0) $\rightarrow CO_2 + H$. Chem Phys Lett 352:281–287

40. Billing GD, Muckerman J, Yu H (2002) Vibrational energy transfer and reactivity in HO + CO collisions. J Chem Phys 117:4755–4760

41. Lakin MJ, Troya D, Schatz GC, Harding LB (2003) A quasiclassical trajectory study of the reaction $OH + CO \rightarrow H + CO_2$. J Chem Phys 119:5848–5859

42. Valero R, Kroes GJ (2004) Theoretical reaction dynamics study of the effect of vibrational excitation of CO on the $OH + CO \rightarrow H + CO_2$ reaction. J Phys Chem A 108:8672–8681

43. Medvedev DM, Gray SK, Goldfield EM, Lakin MJ, Troya D, Schatz GC (2004) Quantum wave packet and quasiclassical trajectory studies of OH + CO: influence of the reactant channel well on thermal rate constants. J Chem Phys 120:1231–1238

44. Valero R, McCormack DA, Kroes GJ (2004) New results for the OH (v = 0, j = 0) + CO (v = 0, j = 0) $\rightarrow H + CO_2$ reaction: five-and full-dimensional quantum dynamical study on several potential energy surfaces. J Chem Phys 120:4263–4272

45. Valero R, van Hemert MC, Kroes GJ (2004) Classical trajectory study of the HOCO system using a new interpolated ab initio potential energy surface. Chem Phys Lett 393:236–244

46. Valero R, Kroes GJ (2004) Role of CO vibration in the complex-forming $OH + CO \rightarrow H + CO_2$ reaction. Phys Rev A: At, Mol, Opt Phys 70:040701

47. He Y, Goldfield EM, Gray SK (2004) Quantum dynamics of vibrationally activated OH–CO reactant complexes. J Chem Phys 121:823–828

48. Valero R, Kroes GJ (2006) Identifying spectator bonds in modeling reactions: $OH + CO \rightarrow H + CO_2$. Chem Phys Lett 417:43–47

49. Garcia E, Saracibar A, Zuazo L, Lagana A (2007) A detailed trajectory study of the $OH + CO \rightarrow H + CO_2$ reaction. Chem Phys 332:162–175

50. Johnson CJ, Poad BL, Shen BB, Continetti RE (2011) Communication: new insight into the barrier governing CO_2 formation from OH + CO. J Chem Phys 134:171106

51. Ma J, Guo H (2011) Full-dimensional quantum state resolved predissociation dynamics of HCO_2 prepared by photodetaching HCO_2^-. Chem Phys Lett 511:193–195

52. Guo H (2012) Quantum dynamics of complex-forming bimolecular reactions. Int Rev Phys Chem 31:1–68

53. García E, Corchado JC, Espinosa-García J (2012) A detailed product distribution analysis of some potential energy surfaces describing the $OH + CO \rightarrow H + CO_2$ reaction. Comput Theor Chem 990:47–52

54. Ruscic B, Schwarz M, Berkowitz J (1989) A photoionization study of the COOH species. J Chem Phys 91:6780–6785

55. Radford H, Wei W, Sears TJ (1992) The rotational spectrum of trans-HOCO and DOCO. J Chem Phys 97:3989–3995

56. Sears TJ, Radford H, Moore MA (1993) b-Dipole transitions in trans-HOCO observed by far infrared laser magnetic resonance. J Chem Phys 98:6624–6631

57. Miyoshi A, Matsui H, Washida N (1994) Detection and reactions of the HOCO radical in gas phase. J Chem Phys 100:3532–3539

58. Ruscic B, Litorja M (2000) Photoionization of HOCO revisited: a new upper limit to the adiabatic ionization energy and lower limit to the enthalpy of formation. Chem Phys Lett 316:45–50

59. McLean A, Ellinger Y (1985) An ab initio configuration interaction study of cis and trans ground-state HOCO radical using localized orbitals: structural analysis or correlation effects. Chem Phys 94:25–41

60. Aoyagi M, Kato S (1988) A theoretical study of the potential energy surface for the reaction $OH + CO \rightarrow CO_2 + H$. J Chem Phys 88:6409–6418

61. Kudla K, Koures AG, Harding LB, Schatz GC (1992) A quasiclassical trajectory study of OH rotational excitation in OH + CO collisions using abinitio potential surfaces. J Chem Phys 96:7465–7473

62. Francisco JS (1997) Molecular structure, vibrational frequencies, and energetics of the HOCO + ion. J Chem Phys 107:9039–9045

63. Duncan TV, Miller CE (2000) The HCO_2 potential energy surface: stationary point energetics and the HOCO heat of formation. J Chem Phys 113:5138–5140

64. Li Y, Francisco JS (2000) High level ab initio studies on the excited states of HOCO radical. J Chem Phys 113:7963–7970

65. Yu HG, Muckerman JT, Sears TJ (2001) A theoretical study of the potential energy surface for the reaction $OH + CO \rightarrow H + CO_2$. Chem Phys Lett 349:547–554

66. Zhu R, Diau E, Lin M, Mebel A (2001) A computational study of the OH (OD) + CO reactions: effects of pressure, temperature, and quantum-mechanical tunneling on product formation. J Phys Chem A 105:11249–11259

67. Song X, Li J, Hou H, Wang B (2006) Ab initio study of the potential energy surface for the $OH + CO \rightarrow H + CO_2$ reaction. J Chem Phys 125:094301

68. Nguyen TL, Xue BC, Weston RE Jr, Barker JR, Stanton JF (2012) Reaction of HO with CO: tunneling is indeed important. J Phys Chem Lett 3:1549–1553

69. Weston RE Jr, Nguyen TL, Stanton JF, Barker JR (2013) HO + CO reaction rates and H/D kinetic isotope effects: master equation models with ab initio SCTST rate constants. J Phys Chem A 117:821–835

70. Senosiain JP, Musgrave CB, Golden DM (2003) Temperature and pressure dependence of the reaction of OH and CO: master equation modeling on a high-level potential energy surface. Int J Chem Kinet 35:464–474

71. Chen WC, Marcus R (2005) On the theory of the CO + OH reaction, including H and C kinetic isotope effects. J Chem Phys 123:094307

72. Senosiain JP, Klippenstein SJ, Miller JA (2005) A complete statistical analysis of the reaction between OH and CO. Proc Combust Inst 30:945–953

73. Li J, Chen J, Zhang DH, Guo H (2014) Quantum and quasi-classical dynamics of the OH + CO → H + CO$_2$ reaction on a new permutationally invariant neural network potential energy surface. J Chem Phys 140:044327

74. Mousavipour SH, Pirhadi F, HabibAgahi A (2009) A theoretical investigation on the kinetics and mechanism of the reaction of amidogen with hydroxyl radical. J Phys Chem A 113:12961–12971

75. Frisch M, Trucks G, Schlegel H, Scuseria G, Robb M, Cheeseman J, Scalmani G, Barone V, Mennucci B, Petersson G (2009) Gaussian 09 (Revision D. 01). Gaussian Inc., Wallingford

76. Grimme S, Antony J, Ehrlich S, Krieg H (2010) A consistent and accurate ab initio parametrization of density functional dispersion correction (DFT-D) for the 94 elements H-Pu. J Chem Phys 132:154104

77. AmE Masunov, Wait E, Vasu SS (2016) Chemical reaction CO + OH → CO$_2$ + H autocatalyzed by carbon dioxide: quantum chemical study of the potential energy surfaces. J Phys Chem A 120:6023–6028

78. Lee TJ, Taylor PR (1989) A diagnostic for determining the quality of single-reference electron correlation methods. Int J Quantum Chem 36:199–207

79. Mazarei E, Mousavipour SH (2018) Theoretical study on the dynamics and kinetics of the reaction of CH$_2$OH with OH. J Phys Chem A 122:9761–9777

80. Chen J, Xu X, Xu X, Zhang DH (2013) Communication: an accurate global potential energy surface for the OH + CO → H + CO$_2$ reaction using neural networks. J Chem Phys 138:221104

81. Barker J, Nguyen T, Stanton J, Aieta C, Ceotto M, Gabas F, Kumar T, Li C, Lohr L, Maranzana A (2017) MultiWell-2017 software suite. University of Michigan, Ann Arbor

82. Gillespie DT (1977) Exact stochastic simulation of coupled chemical reactions. J Phys Chem 81:2340–2361

83. Gillespie DT (1992) A rigorous derivation of the chemical master equation. Phys A 188:404–425

84. Robinson PJ, Holbrook KA (1972) Unimolecular reactions. Wiley Interscience, New York

85. Forst W (1973) Theory of unimolecular reactions. Academic Press, New York

86. Gilbert RG, Smith SC (1990) Theory of unimolecular and recombination reactions. Blackwell Scientific, Oxford

87. Baer T, Hase WL, William L (1996) Unimolecular reaction dynamics: theory and experiments. Oxford University Press on Demand, New York

88. Albert J (2016) A hybrid of the chemical master equation and the Gillespie algorithm for efficient stochastic simulations of sub-networks. PLoS ONE 11:e0149909

89. Frankcombe TJ, Smith SC, Gates KE, Robertson SH (2000) A master equation model for bimolecular reaction via multi-well isomerizing intermediates. Phys Chem Chem Phys 2:793–803

90. Eckart C (1930) The penetration of a potential barrier by electrons. Phys Rev 35:1303

91. Johnston HS, Heicklen J (1962) Tunnelling corrections for unsymmetrical Eckart potential energy barriers. J Phys Chem 66:532–533

92. Johnston HS (1966) Gas phase reaction rate theory. Ronald Press Co., New York

93. Stein SE, Rabinovitch B (1973) Accurate evaluation of internal energy level sums and densities including anharmonic oscillators and hindered rotors. J Chem Phys 58:2438–2445

94. Beyer T, Swinehart D (1973) Number of multiply-restricted partitions. Commun ACM 16:379

95. Hippler H, Troe J, Wendelken H (1983) Collisional deactivation of vibrationally highly excited polyatomic molecules. II. Direct observations for excited toluene. J Chem Phys 78:6709–6717

96. Johnson CJ, Continetti RE (2010) Dissociative photodetachment studies of cooled HOCO⁻ anions revealing dissociation below the barrier to H + CO$_2$. J Phys Chem Lett 1:1895–1899

97. Dean A (1985) Predictions of pressure and temperature effects upon radical addition and recombination reactions. J Phys Chem 89:4600–4608

98. Zhu L, Hase W (1993) A general RRKM program (QCPE 644). University of Indiana, Bloomington

99. Börjesson L, Nordholm S (1995) Microcanonical correlation analysis of collisional energy transfer efficiencies in unimolecular reactions. J Phys Chem 99:938–944

100. Tardy D, Rabinovitch B, Whitten G (1968) Vibration-rotation energy-level density calculations. J Chem Phys 48:1427–1429

101. Brown R (1981) A method of calculating tunneling corrections for Eckart potential barriers. J Res Natl Bur Stand 86:357–359

102. Hirschfelder J, Wigner E (1939) Some quantum-mechanical considerations in the theory of reactions involving an activation energy. J Chem Phys 7:616–628

103. Miller WH (1976) Unified statistical model for complex and direct reaction mechanisms. J Chem Phys 65:2216–2223

104. Garrett BC, Truhlar DG (1982) Canonical unified statistical model. Classical mechanical theory and applications to collinear reactions. J Chem Phys 76:1853–1858

105. Zheng J, Bao J, Meana-Pañeda R, Zhang S, Lynch B, Corchado J, Chuang Y, Fast P, Hu W, Liu Y (2016) POLYRATE (version 2016-2A). University of Minnesota, Minneapolis